The use of 3D EM simulators in the time domain for phased array applications

Phased array antennas are planar double-periodic structures that find many applications in electronic systems. One of the methods of analysing complex phased arrays is to assume that the array is infinite by only considering a single unit-cell model. This paper describes the advantages and method of application of the finite integration technique (FIT) to infinite array analysis.

In computer science, the concept of "divide and conquer" is an important paradigm for algorithm design. It implies the recursive breaking down of a problem into two or more sub-problems of the same (or related) type, until these become simple enough to be solved directly. The solutions to the sub-problem are then combined to give a solution to the original problem.

Phased array antennas are planar double-periodic structures that find many applications in electronic systems. One of the methods of analysing complex phased arrays is to assume that the array is infinite by only considering a single unit-cell model. The infinite array idealisation of antenna arrays is a powerful analysis tool. Although it neglects edge effects, it provides the essential design parameters for large antenna arrays. The application of FIT offers many advantages:

- Complicated geometries and materials can be analysed, where no analytic Green's functions for a method of moment technique are available
- The FIT is a general tool that avoids the need to develop new codes for new radiators,
- Since only one unit cell with phase shift walls is analysed, the model size fits the computational capabilities of present PCs and drastically reduces runtimes.

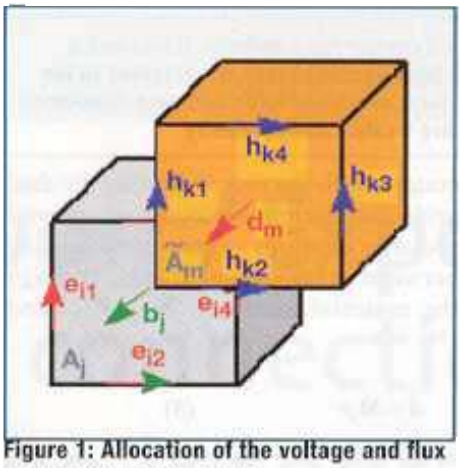

Figure 1: Allocation of the voltage and flux components in the mesh

The analysis of phased-array antennas has been an important research and design area for the last couple of decades. Till now the main numerical tool for analysing phased-array radiating elements was the MOM [1]. It deserved the development of specific codes for the different types of elements used in phased arrays, dipoles, open waveguides, notches, slots, micro-strips, etc. As phased array antennas progresses the geometrical complexity of the design, the use of new dielectric materials and the demand for monolithic designs all raise the need for a general tool that would be able to analyse any phased-array radiating element.

In response, CST is taking up the challenge of implementing leading-edge technology, providing versatility and increasing usability with the development of Version 5 of CST Microwave Studio (CST MWS). Based on a long software history, the very general theoretical approach reveals its full power in the wide range of applicability, covering static and low frequency applications (via CST EM Studio) to the highest frequencies in the optical regime.

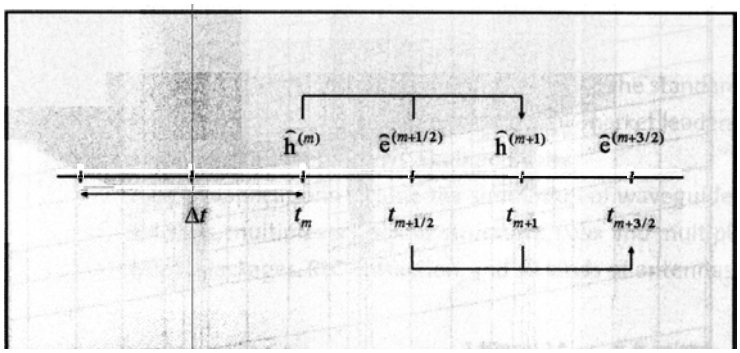

Figure 2: The leap-frog scheme

Numerical Techniques

In this section, the numerical techniques employed for the 3D field simulation and for the subsequent determination of the far field and S-parameters are briefly described.

The Finite Integration Technique

The numerical method used for the field simulation is the Finite Integration Technique (FIT), first proposed by Weiland in 1977 [2]. FIT generates exact algebraic analogues to Maxwell's equations, which guarantee that the physical properties of fields are maintained in the discrete space, and lead to a unique solution. Maxwell's equations and the related material equations are transformed from the continuous to the discrete space by allocating electric voltages on the edges of a grid G, and magnetic voltages on the edges of a dual grid $\tilde{G}$,.

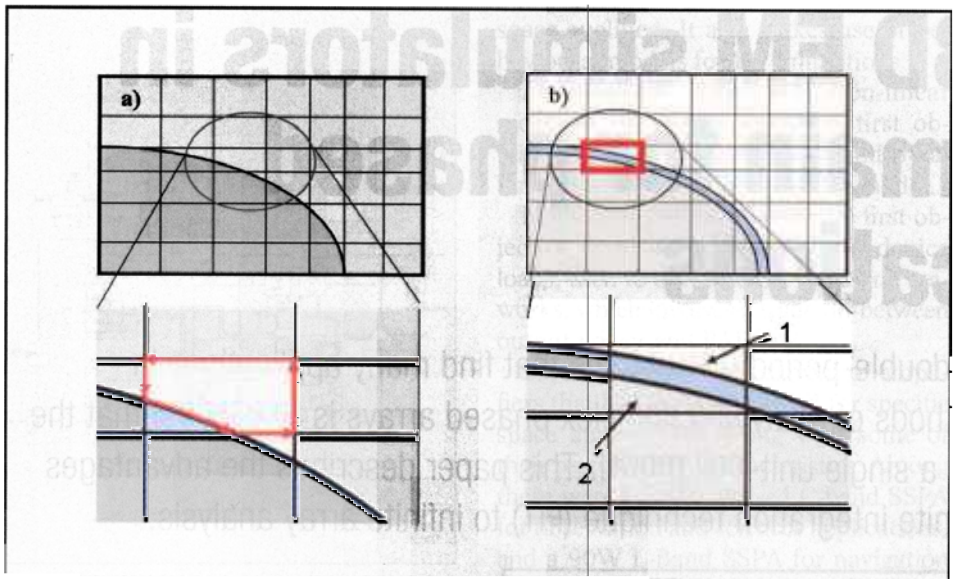

Figure 3(a), left: Illustration of PBA for a mesh cell containing a metallic (blue) and a dielectric part (grey), the contour path integrals (highlighted in red) are adjusted to the actual cell. Figure 3(b), right: Illustration of TST for a mesh cell filled with two dielectrics separated by a metallic sheet - regions 1 and 2 are treated independently

The allocation of the voltage and flux components on the grid can be seen in Figure 1. The use of integral degrees of freedom, i.e. voltages and fluxes, instead of field components (as used in FDTD) allows not only a very elegant way of writing the matrix equations (1 - 4), but also has important algorithmic-theoretical and numerical consequences [3]. The discrete equivalent of Maxwell's equations, the so-called Maxwell's Grid Equations are shown in Equations (1) - (4). This description is still an exact representation and does not contain any approximation errors.

$$\mathbf{C}\hat{\mathbf{e}} = -\frac{d}{dt}\hat{\tilde{\mathbf{b}}} \qquad (1)$$

$$\tilde{\mathbf{C}}\hat{\mathbf{h}} \quad \frac{d}{dt}\hat{\tilde{\mathbf{d}}} + \qquad (2)$$

$$\mathbf{S}\hat{\mathbf{b}} = 0 \qquad (3)$$

$$\tilde{\mathbf{S}}\hat{\mathbf{d}} = \mathbf{q} \qquad (4)$$

In these equations $\hat{\mathbf{e}}$ and $\hat{\mathbf{h}}$ denote the electric and magnetic voltages along primary and dual edges, respectively.

The symbols $\hat{\tilde{\mathbf{a}}}$, $\hat{\tilde{\mathbf{b}}}$ and $\hat{\tilde{\mathbf{j}}}$ are the electric, magnetic, and current-density fluxes across primary and dual grid faces. The topological matrices $\mathbf{C}$, $\tilde{\mathbf{C}}$, $\mathbf{S}$ and $\tilde{\mathbf{S}}$ represent the discrete equivalents of the curl- and the div-operators, with the tilde indicating the dual grid. The discrete analogues of material property relations express the coupling between voltages and fluxes, through the material matrices $\mathbf{M}_\varepsilon$, $\mathbf{M}_{\mu^{-1}}$ and $\mathbf{M}_\sigma$

$$\hat{\tilde{\mathbf{d}}} = \mathbf{M}_\varepsilon \hat{\mathbf{e}} \qquad (5)$$

$$\hat{\mathbf{h}} = \mathbf{M}_{\mu^{-1}} \hat{\tilde{\mathbf{b}}} \qquad (6)$$

$$\hat{\tilde{\mathbf{j}}} = \mathbf{M}_\sigma \hat{\mathbf{e}} + \hat{\tilde{\mathbf{j}}}_A \qquad (7)$$

These matrices have diagonal form and contain the unavoidable approximations of any numerical procedure. FIT can be applied to different frequency ranges, from DC to THz. On Cartesian grids, the time-domain FIT can be rewritten to yield the FDTD scheme. However, whereas the classical FDTD has the disadvantage of the staircase approximation of complex boundaries, the Perfect Boundary Approximation (PBA) [4] technique applied in conjunction with FIT maintains all the advantages of the structured Cartesian grids, while allowing an accurate modelling of curved boundaries.

The boundary of the calculation domain is assumed to be ideal electric, ideal magnetic or 'open'. The perfectly matched layer (PML) [5] is used in the case of open boundaries.

■ Time domain simulation

The time-domain FIT is the most efficient scheme for many RF-applications. For the discretisation of the time derivative, the well-known explicit leap-frog algorithm is used. It is very memory-efficient and has the advantage that the calculation of the unknowns at each time step only requires one matrix-vector multiplication (linear complexity). This scheme is illustrated in Figure 2. FIT in time domain is therewith a generalisation of the FDTD method [6].

The excitation signal for the time domain calculation can be fed in the structure on any desired path of edges in the primary grid. This path is referred to as discrete port. More complex waveguide structures are excited with a so-called waveguide port. For the computation of S-parameters, one or many discrete or waveguide ports are defined in the computational domain or at its boundary, respectively. To obtain a full S-parameter matrix, all ports are excited successively with an appropriate time-domain pulse, and the output (reflected or transmitted) signals at all further ports are recorded.

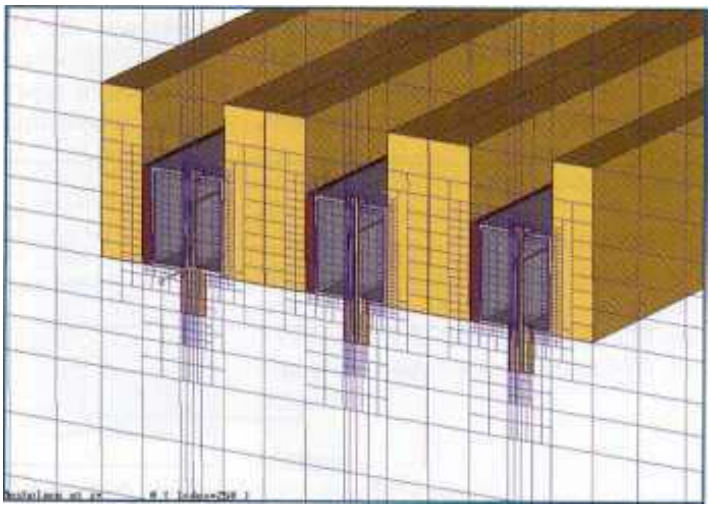

Figure 4: A waveguide-fed slot-antenna meshed with MSS, where the refinement takes place on several layers which run conformally along the structure, gaining a 4-fold reduction of mesh cells for the same resolution.

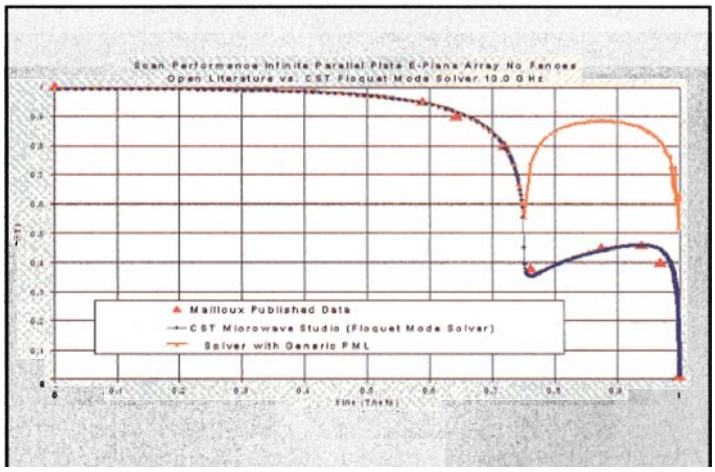

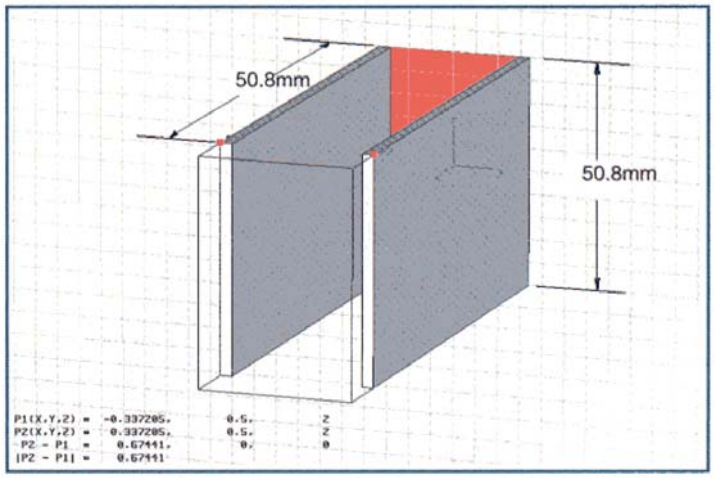

Figure 5(a), left: Power transmission factor of a parallel plate array - the Floquet mode solver allows the user to distinguish between main radiating mode and grating lobe, and Figure 5(b), right: dimensions of parallel plates

To calculate the S-parameters over a wide range of frequencies, a broadband input signal is chosen, typically a Gaussian modulated sine function.

All the input and output signals resulting from the time domain simulation are then transformed into the frequency domain by application of a Discrete Fourier Transform (DFT) algorithm. Finally, the S-parameters are obtained as the ratio of these frequency domain representations of the direct incident and inverse wave components.

■ Meshing Strategies

The performance of the broadband time domain simulation depends on the number of grid cells and the coarseness of the grid, while the accuracy often depends on the geometry approximation of the structure on the grid. Therefore a meshing method that optimises all three requirements is preferable.

Whereas the classical FDTD has the disadvantage of the staircase approximation of complex boundaries, the Perfect Boundary Approximation (PBA) [4] technique applied in conjunction with FIT maintains all the advantages of the structured Cartesian grids, i.e. high memory efficiency and simulation speed, while allowing an accurate modelling of curved boundaries (Figure 3a) and a provably better convergence. In particular metallisation planes can be considered with their finite thickness without explicit discretisation.

An extension to PBA is the Thin Sheet Technique (TST), this enables the accurate treatment of arbitrarily shaped housings or inclined thin metallic sheets (Figure 3b). These techniques provide a precise representation of geometry within one grid cell, thus allowing a comparatively coarse grid for the computation.

The performance of the simulation can also be improved by reducing the sheer number of mesh cells by applying a subgridding scheme. The Multilevel Subgridding Scheme (MSS) is an optimal approach, because it covers the volume to be refined with conformal layers of increasingly finer mesh, excluding perfectly electric conducting regions from simulation at the same time (Figure 4).

■ Frequency Domain

FIT is not restricted to Time Domain simulations; it can also be formulated in the Frequency Domain, where the treatment of periodic structures particularly important in phased array technology, is very handy.

In CST MWS a periodic (Floquet mode) boundary port mode solver is implemented that delivers highest accuracy for wide radiation angles, especially for phased array calculations. It is here applied to a parallel plate waveguide array [7]. The Floquet Mode solver allows the separation of the grating lobe from the

Figure 6, (left): TerraSAR X antenna, and Figure 7, (right): Photograph of one panel with its 32 subarrays

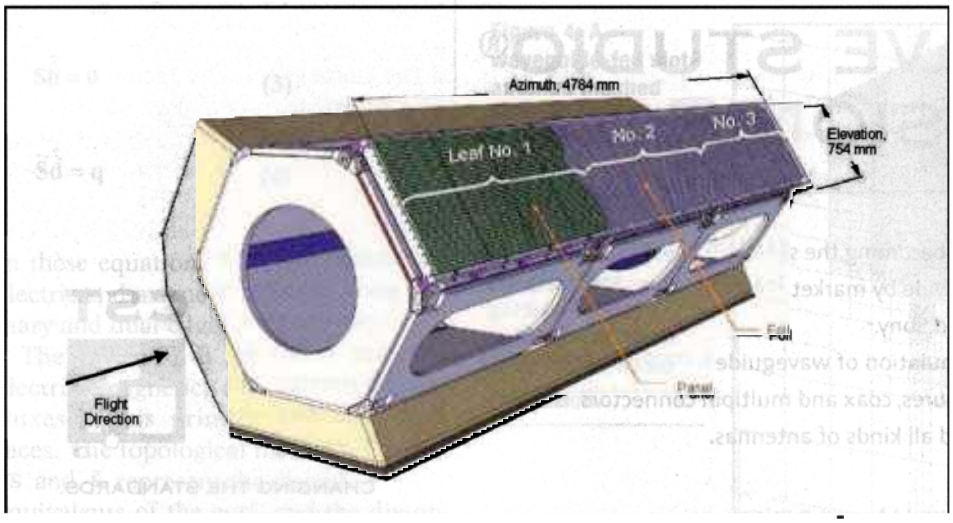

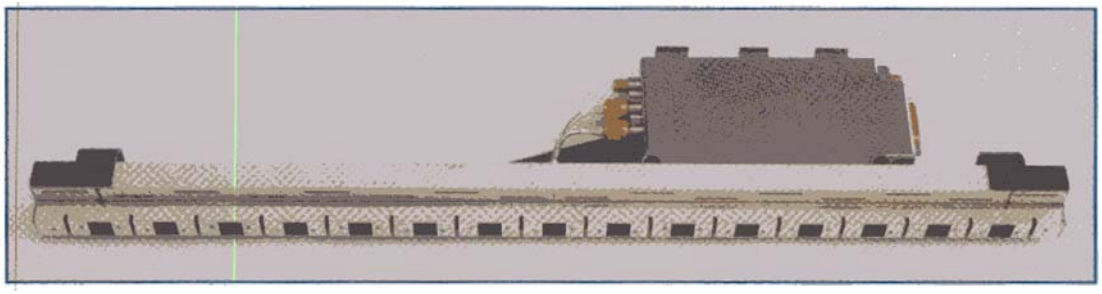

Figure 8: Subarray of the T/R module

main radiating mode, thus allowing the direct specification of the power transmission factor for the principal mode (Figure 5).

Since the plane wave is also a solution of the periodic boundary port, the illumination of Frequency Selective Surfaces (FSS) under arbitrary angle can be easily done.

Maxwell's Grid Equations in time harmonics, driven by imprinted (displacement) currents can be expressed as the following:

$$\mathbf{C}\hat{\mathbf{e}} = -\mathrm{j}\omega\hat{\mathbf{b}} = -\mathrm{j}\omega\underline{\mathbf{M}}_{\mu}\hat{\mathbf{h}} \qquad (8)$$

$$\tilde{\mathbf{C}}\hat{\mathbf{h}} = \mathrm{j}\omega\hat{\tilde{\mathbf{d}}} + \hat{\tilde{\mathbf{j}}} + \hat{\tilde{\mathbf{j}}}_{\mathrm{i}} = \mathrm{j}\omega\underline{\mathbf{M}}_{\varepsilon}\hat{\mathbf{e}} + \mathrm{j}\omega\mathbf{M}_{\varepsilon}\hat{\mathbf{e}}_{\mathrm{i}} \qquad (9)$$

$$\mathbf{S}\hat{\tilde{\mathbf{b}}} = 0 \qquad (10)$$

$$\tilde{\mathbf{S}}\hat{\tilde{\mathbf{d}}} = 0 \qquad (11)$$

finally leading to the curl-curl equation which has to be solved by e.g. Modified-Krylov-Subspace Method:

$$\tilde{\mathbf{C}}\underline{\mathbf{M}}_{\nu}\mathbf{C}\hat{\mathbf{e}} - \omega^2\underline{\mathbf{M}}_{\varepsilon}\hat{\mathbf{e}} = \omega^2\mathbf{M}_{\varepsilon}\hat{\mathbf{e}}_{\mathrm{i}} \qquad (12)$$

The depending degrees of freedom of the electric fields E are linked to the independent ones obeying the equation

$$\mathbf{E}_{\mathrm{dep}} = \mathrm{e}^{\mathrm{j}\phi}\cdot\mathbf{E}_{\mathrm{indep}} \qquad (13)$$

and are eliminated from the equation system. The relation between the electrical phase shift ξ_x, ξ_y and the scan direction is given by:

$$\xi_x = \mathbf{k}\mathbf{d}_x \sin\theta_s \cos\varphi_s \qquad (14)$$

$$\xi_y = \mathbf{k}\mathbf{d}_y \sin\theta_s \cos\varphi_s \qquad (15)$$

Practical example

TerraSAR-X [8,9] is an X-band Synthetic Aperture Radar developed by the German Aerospace Centre (DLR) and EADS Astrium GmbH. TerraSAR-X features a full polarimetric active phased array antenna with 384 T/R modules.

With respect to cost-effective manufacturing, two kinds of waveguide radiators are used for horizontal (HP) and vertical (VP) polarisation. Around the centre frequency of 9.65GHz, a bandwidth of up to 300MHz is possible.

The TerraSAR-X antenna and its accommodation on the space-craft is shown in Figure 6. The antenna consists of three 'leaves', each leaf grouping four 'panels'. A panel is made up of 32 subarrays, each comprising an HP and a VP slotted waveguide radiator (Figure 7). Horizontal polarisation is oriented parallel to azimuth (flight) direction, vertical polarisation parallel to the elevation direction, respectively. Each of the 32 x 12 = 384 subarrays is equipped with a T/R module.

A close-up view of one subarray is shown in Figure 8. In the back, the T/R module with the connectors for both polarisations and a third (unconnected) calibration port can be seen. In the front, the two waveguide radiators are visible, with HP being the lower one (vertical slots) and VP the upper one.

For verification purposes only three subarrays are mounted in a test jig and measured for vertical polarisation as shown in Figure 9.

The simulation model (Figure 10) is identical to the test jig, except the missing absorbers in the horizontal plane, and is completely enclosed by open boundaries. The excitation signals through the coaxial ports have the same magnitude and a phase of 0° for comparison reason with measurements. The 3D far-field pattern of Figure 11 shows a maximum directivity equal to 24.67dBi, while the measurement shows 25.28dBi. A curve overlay can be performed (scaling both curves to a maxi-

Figure 9, (right): Test jig for subarray measurements consisting of three T/R modules

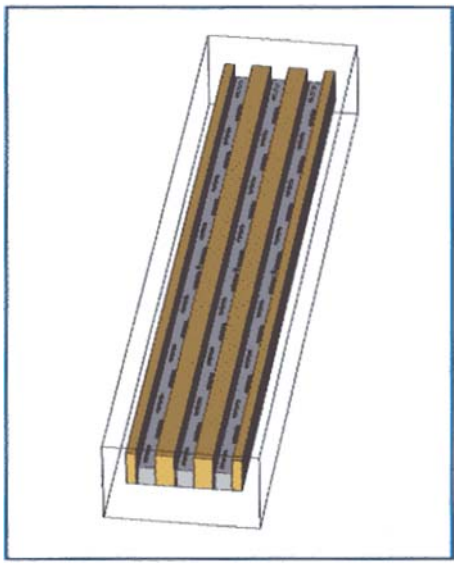

Figure 10, (far right): The CST MWS model is completely embedded in open boundaries at the periphery

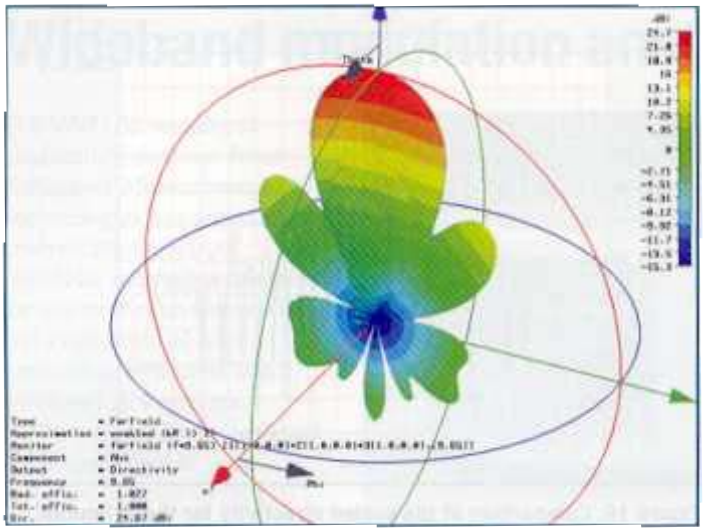

Figure 11: 3D far-field pattern of the directivity for simultaneous excitation, phase offsets are zero

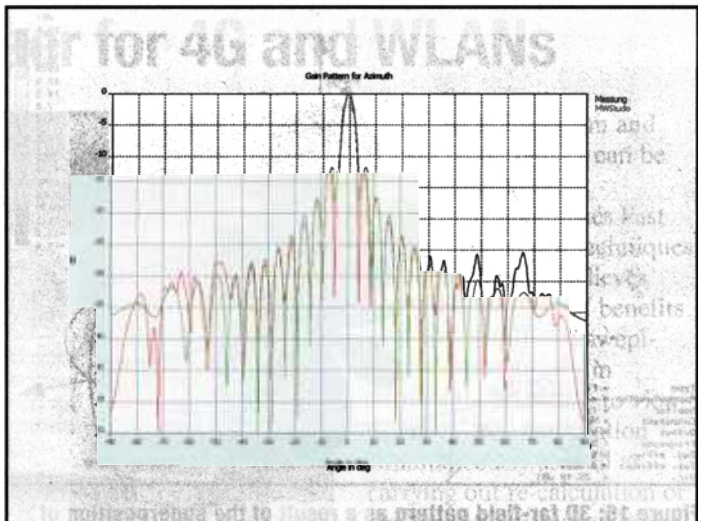

Figure 12: Comparison measurement vs. simulation for the azimuthal cut

mum of 0dBi) thus enabling a direct graphical comparison (Fig 12). The direction of the side-lobes is in excellent agreement, however, the level deviates by about 1dBi at a level of -12dBi caused by the missing absorber mates in the simulation model.

To study the impact of variable array-sizes with respect to the farfield and to reduce runtime, a single T/R 'submodule' (unit cell) may be used for simulation purposes.

The simulation model thus only consists of a single subarray (unit cell) with assumed phase-shift of zero degrees at the periodic boundaries. Figure 13 shows a close-up of the simulation model at the feeding details for the slotted waveguide. The far field of the unit cell model is superimposed with the proper geometrical offset (Figure 14) and a possible phase shift unequal to zero resulting in total far-field pattern plotted in Figure 15. The agreement is excellent in a range of ±40°, also the magnitude differs by only 0.2dBi at an absolute level of about 26dBi at boresight (Figures 16 and 17). The elevation cut shows a slight asymmetry due to the unsymmetrical placement of the HP waveguides.

The vertical periodic boundaries simulate the infinite extension of the antenna array, thus the measured S-parameters for an array consisting of a sufficiently large number of subarrays can be compared with the simulated ones.

In Figure 18 both S-parameters are shown. The shape and magnitude are in excellent agreement, the frequency shift is in the range of 1% related to the centre frequency of 9.65GHz. The run-time for the unit cell model (containing 380,000 mesh cells) on a Xeon-PC (2.66GHz) was about 48 minutes.

Conclusion

This paper began with the fundamentals of the Finite Integration Technique, and discussed the latest developments to further improve accuracy and efficiency of the method. It was pointed out that FIT is a general approach that allows the user to choose between different methods (Frequency and Time Domain) and meshes in order to approach this problem as efficient as possible. All the features and techniques that have been introduced are implemented in the commercial software CST Microwave Studio. By showing a complex radar application, the versatility and usability of the software in the area of phased arrays is demonstrated, measurements and simulation results are in excellent agreement.

Acknowledgment

The author would like to thank the company EADS Astrium GmbH for the models, measurements and its support of this

Figure 13, (right): Close-up look at the feed of the simulation model32. The vertical sidewalls are defined as periodic boundaries of phase shift equal to zero

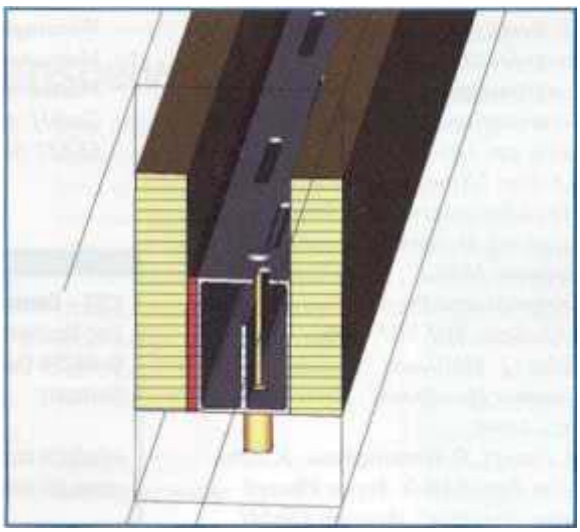

Figure 14, (far right): The pop-up menu for the superposition of far fields, showing the setup for the three subarrays with a given mechanical offset and a phase offset of 0°

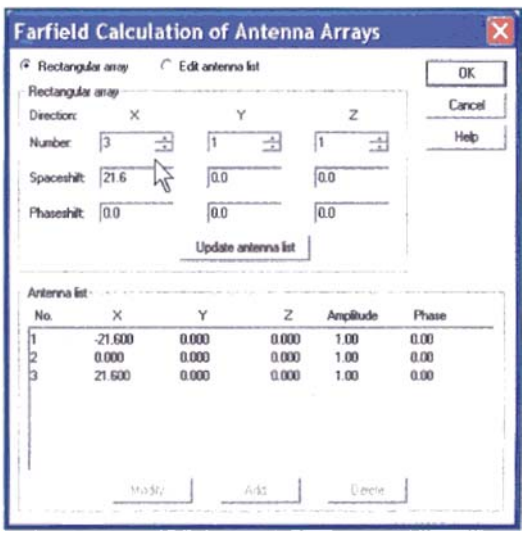

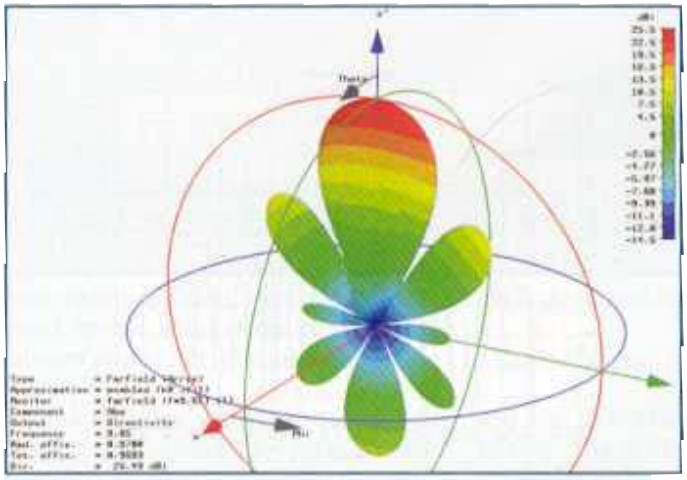

Figure 15: 3D far-field pattern as a result of the superposition of the unit cell pattern: the deviation is only 0.2dBi compared to measurement

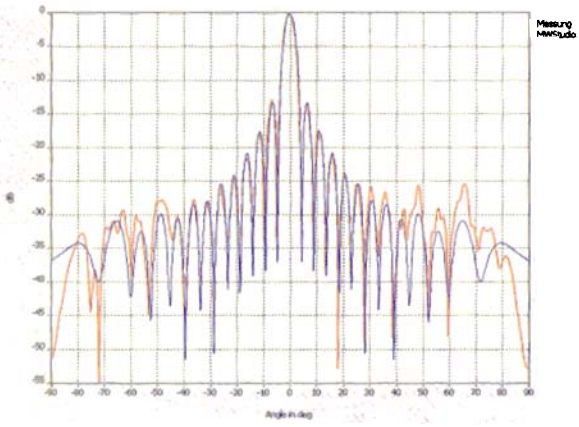

Figure 16: Comparison of the scaled directivity for the azimuthal cut plane: in the range of ±40° the agreement is excellent

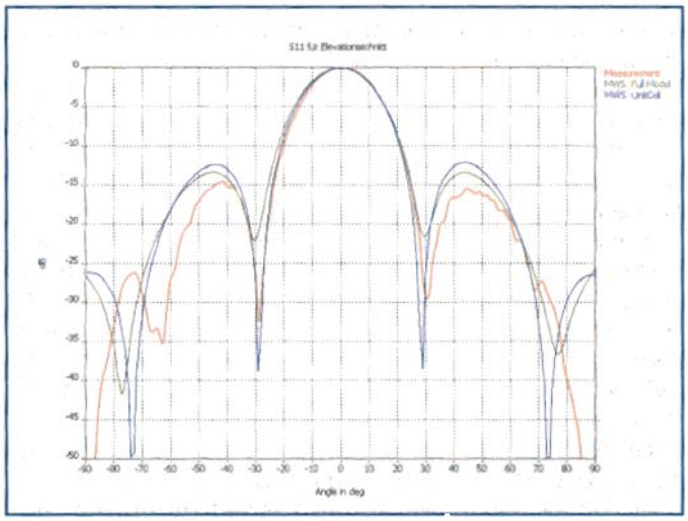

Figure 17: Comparison of measurement and simulation for the elevation cut

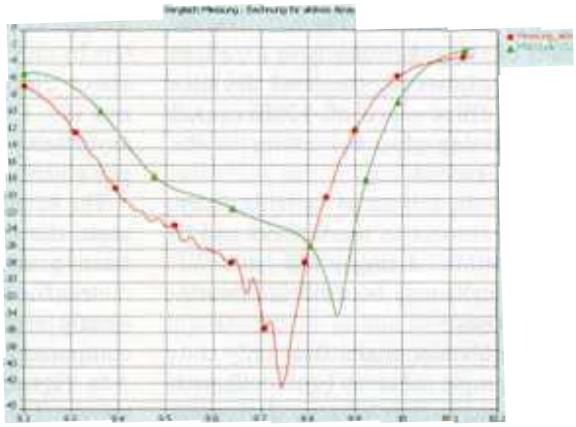

Figure 18: Comparison of the active reflection parameter S11

paper.

References

[1] *Amitai, Galindo and Wu: "Theory and Analysis of Phased Array Antennas", Wiley, 1972*

[2] *T. Weiland: "A Discretisation Method for the Solution of Maxwell's Equations for Six-Component Fields", Electronics and Communication 31, Page 116, 1977*

[3] *T. Weiland, "Time Domain Electromagnetic Field Computation with Finite Difference Methods", International Journal of Numerical Modelling, Vol. 9, pp. 295-319 (1996).*

[4] *B. Krietenstein, R. Schumann, P. Thoma, T.Weiland: "The Perfect Boundary Approximation Technique Facing the Big Challenge of High Precision Field Computation", Proc. Of the Int. Linear Accelerator Conference, Chicago, USA, 1998, pp. 860-862*

[5] *J.P. Berenger, "A Perfectly Matched Layer for the Absorption of Electromagnetic Waves", Journal of Computational Physics, Vol. 114, 1994, pp. 185-200.*

[6] *K.S.Yee: "Numerical Solution of Initial Boundary Value Problems Involving Maxwell's Equations in Isotropic Media", IEEE Trans. On Antennas and Propagation, Band 14, Nr.3, Seite 302-307, 1966*

[7] *Robert J. Mailloux, "Phased Array Antenna Handbook", Artech House Inc., 1994*

[8] *M. Stangl, R.Werninghaus, R.Zahn: "The TerraSAR-X Active Phased Array Antenna", Astrium GmbH, 88039 Friedrichshafen, DLR German Aerospace Center, 53227 Bonn*

[9] *A. Herrschlein, C. Fischer, H. Baumann, M.Stangl, W. Pitz, R. Werninghaus: "Development and Measurement Results for TerraSAR-X Phased Array", EADS Astrium GmbH, 88039 Friedrichshafen, DLR, 53227 Bonn*

AUTHORS INFORMATION

CST - Computer Simulation Technology
Bad Nauheimer Strasse 19
D-64289 Darmstadt
Germany

info@cst.com
www.cst.com